Dynamic Deformation and Recovery Response of Red Blood Cells to a Cyclically Reversing Shear Flow: Effects of Frequency of Cyclically Reversing Shear Flow and Shear Stress Level

Nobuo Watanabe,* Hiroyuki Kataoka,* Toshitaka Yasuda,† and Setsuo Takatani*
*Department of Artificial Organs, Institute of Biomaterials and Bioengineering, Tokyo Medical and Dental University, Tokyo, Japan; and †Graduate School of Medicine, Yamaguchi University, Yamaguchi, Japan

ABSTRACT Dynamic deformation and recovery responses of red blood cells (RBCs) to a cyclically reversing shear flow generated in a 30-μm clearance, with the peak shear stress of 53, 108, 161, and 274 Pa at the frequency of 1, 2, 3, and 5 Hz, respectively, were studied. The RBCs' time-varying velocity varied after the glass plate velocity without any time lag, whereas the L/W change, where L and W were the major and minor axes of RBCs' ellipsoidal shape, exhibited a rapid increase and gradual decay during the deformation and recovery phase. The time of minimum L/W occurrence lagged behind the zero-velocity time of the glass plate (zero stress), and the delay time normalized to the one-cycle duration remained constant at 8.0%. The elongation of RBCs at zero stress time became larger with the reversing frequency. A simple mechanical model consisting of an elastic linear element during a rapid elongation period and a parallel combination of elements such as a spring and dashpot during the nonlinear recovery phase was suggested. The dynamic response behavior of RBCs under a cyclically reversing shear flow was different from the conventional shape change where a steplike force was applied to and completely released from the RBCs.

INTRODUCTION

The deformability of red blood cells (RBCs) under shear flow has been studied during the last 30 years to understand the biomechanical capability of RBCs in circulatory dynamics. The RBCs with a mean diameter of 8 μm subjected to a randomly varying shear stress in the cardiac chamber and larger vessels must flexibly alter their shape to pass through 3- to 4-μm-diameter capillaries of the microcirculation (1) as oxygen carriers. The ability of RBCs to deform and maintain the oxygen-carrying capability under a randomly varying shear flow is of great interest from the standpoint of rheological and functional behavior of RBCs in the cardiovascular system.

Previous studies have uncovered various findings related to the deformability of RBCs in a steady, uniform shear-flow field. These included the ellipsoidal shape in a high shear flow (2), the rotation of the RBC membrane, called tank-treading motion, the effect of shear-stress amplitude on elongation, the effect of shear rate on the rotational speed of tank-treading motion (3–5), the effect of internal and external viscosity ratio and membrane stiffness and hematocrit on deformability (6,7). Theoretical models have also been published (8–13) that describe the deformation mechanism of RBCs in the uniform shear flow. Many experimental studies have been performed to understand hemolysis (14) with respect to a specific uniform shear-stress level and exposure time (15–17). Consequently, the mathematical relations between the uniform shear-stress level and hemolysis of RBCs have also been reported (18,19). In addition, works by Nevaril and Velker (20,21) on morphological changes and/or decrease in cell deformability caused by various levels of shear stress suggested that affected blood cells might clog up the microvessels, leading to tissue infarction, or might be filtered by the spleen function (22). In addition, fluctuating shear flow under a normal physiological condition (peak shear stress $<$3.0 Pa) has also been addressed (23,24).

The study of RBCs has also extended to the analysis and design of cardiovascular devices such as heart-lung bypass systems to minimize mechanical effects that cause hemolysis. In relation to hemolysis, Bludszuweit predicted that the shear-stress fluctuation would exceed 100 Pa along the streamline inside commercially available centrifugal blood pumps (25,26). The randomly fluctuating shear flow generated inside the cardiovascular devices is expected to induce a large transmembrane stress and to cause rupture of the RBC membrane. How RBCs deform and withstand rupture in a fluctuating shear-flow field is of great interest for biomedical researchers to minimize mechanical trauma to RBCs in cardiovascular devices. The deformation capability of RBCs subjected to a cyclically reversing shear flow with high peak shear stress that simulates a randomly varying condition has not yet been studied.

This study was thus designed to provide both experimental and theoretical insight into the deformation and recovery process of normal human RBCs subjected to a cyclically

Submitted January 26, 2006, and accepted for publication June 1, 2006.

Address reprint requests to Prof. Setsuo Takatani, Dept. of Artificial Organs, Institute of Biomaterials and Bioengineering, Tokyo Medical and Dental University, 2-3-10 Surugadai, Kana, Chiyoda-ku, Tokyo, Japan 101-0062. Tel.: 81-3-5280-8168; Fax: 81-3-5280-8168; E-mail: takatani.ao@tmd.ac.jp.

Dr. Hiroyuki Kataoka's present address is RIKEN, Wako Institute, Saitama, Japan.

0006-3495/06/09/1984/15 $2.00

doi: 10.1529/biophysj.105.060236

reversing shear flow that simulated the randomly varying high shear field of various cardiovascular devices. To attain this goal, we built a cyclically reversing shear-flow generator (CRSFG) that could generate one-dimensional, cyclically reversing shear flow with its peak shear stress exceeding 100 Pa (27,28). The time course of deformation and recovery behavior of normal fresh human RBCs was studied to possibly uncover dynamic mechanical responses to a cyclically reversing shear flow.

MATERIALS AND METHODS

Theory of oscillatory Couette flow between two parallel glass plates

First of all, the oscillatory Couette flow condition was a key in designing an experimental system. We designed a system that could exert an equal level of cyclically fluctuating shear stress to all the RBCs inside the flow field. The experimental system is described in the following section. In this section, the theory of a reversing Couette flow is reviewed (29).

Assuming a viscous fluid between the two parallel plates, and considering a flow created by an oscillatory motion of the upper plate, Eq. 1 shows a governing equation for the flow velocity u between the two glass plates,

$$\frac{\partial u}{\partial t} = \nu \frac{\partial^2 u}{\partial^2 y^2}, \quad (0 < y < h), \tag{1}$$

where $\nu = \mu/\rho$ and μ and ρ are the viscosity and density, respectively, of the fluid. Boundary conditions at $y = 0$ and h are given by Eqs. 2 and 3 below.

$$y = 0: u = U \cos \omega t \,(\text{on the surface of the moving upper plate}) \tag{2}$$

$$y = h: u = 0 \,(\text{on the stationary bottom plate surface}). \tag{3}$$

Here, h is the clearance width between the two parallel plates. Equation 2 indicates that at $y = 0$, flow is a sinusoidal function of the angular velocity ω. Equation 1 has a solution in the following form:

$$u = (Ae^{\lambda y} + Be^{-\lambda y})e^{i\omega t}, \quad \lambda = (1+i)k, \quad k = \left(\frac{\omega}{2\nu}\right)^{1/2}. \tag{4}$$

Using boundary conditions (Eqs. 2 and 3), arbitrary constants A and B can be determined to yield the solution:

$$u = U\frac{\sinh\lambda(h-y)}{\sinh\lambda h}e^{i\omega t}. \tag{5}$$

Consequently, the frictional force is given by the following equation:

$$\tau_{yx} = \mu\frac{\partial u}{\partial y} = -\mu U y\frac{\cosh\lambda(h-y)}{\sinh\lambda h}e^{i\omega t}. \tag{6}$$

We define the frictional stresses on the bottom and upper plates as τ_+, τ_-:

$$\tau_- = (\tau_{yx})_{y=0} = -\mu U\lambda \coth\lambda h e^{i\omega t} \tag{7}$$

$$\tau_+ = -(\tau_{yx})_{y=h} = \mu U\lambda \,\mathrm{cosech}\lambda h e^{i\omega t} = -\frac{\tau_-}{\cosh\lambda h}. \tag{8}$$

When the thickness of the boundary layer is larger than the clearance width between the two parallel plates, the following relation can be derived from Eq. 5:

$$u \approx U\left(1 - \frac{y}{h}\right)e^{i\omega t}, \quad h \ll \left(\frac{\nu}{\omega}\right)^{1/2}. \tag{9}$$

Equation 9 indicates that the flow profile is laminar and Couette at any moment. Then Eqs. 6–8 reduce to Eq. 10 below.

$$\tau_{yx} = -\frac{\mu U}{h}e^{i\omega t}, \quad \tau_- = -\tau_+ = -\frac{\mu U}{h}e^{i\omega t}. \tag{10}$$

In this study, we designed the experimental system to satisfy the conditions of Eq. 9 and to produce an oscillatory Couette flow. The clearance width h of 30 μm between the parallel plates, kinematic viscosity of the fluid ν of 1.82×10^{-4} m^2/s and fluid density ρ of 1100 kg/m^3 at the temperature of 24.5°C satisfied the relation shown in Eq. 9.

Preparation of human RBC-dextran PBS

Phosphate-buffered solution (PBS) was first prepared by dissolving a PBS powder (Wako Pure Chemical Industries, Osaka, Japan) in the distilled water. The dextran powder, with a molecular weight of 60,000–90,000 (dextran, low fraction, Acros Organics, Fairlawn, NJ) was mixed into the PBS with the weight percentage of 31, and then kept for few days in the refrigerator for better mixing. The viscosity of the dextran PBS was 0.20 Pa s at 24.5°C as measured using a rotating viscometer (DV-II Pro, Brookfield Engineering Laboratories, Middleboro, MA).

A 10-μl amount of fresh human whole blood was collected into an anticoagulated glass tube (Vitrex 1771, Modulohm A/S, Herlev, Denmark) by needle puncture from the fingertip of a healthy male volunteer and mixed with 1.0 ml of dextran PBS. The hematocrit of the RBC-dextran PBS was 0.45 vol %, and its viscosity was the same as that of the dextran PBS.

Cyclically reversing shear flow generator and microscope data acquisition system

Fig. 1 showed the schematic diagram of the experimental set-up that consisted of a CRSFG and a microscope data acquisition system. The arm of the slider-crank mechanism that was linked to the eccentric cam-motor system was attached to the upper movable plate of the parallel glass plate assembly (PGPA) between which the RBC suspension was inserted. Fig. 2 showed the assembled CRSFG system.

Two pieces of stainless steel spacer each having a thickness of 30 μm, a width of 12.7 mm, and a length of 150 mm (FGSM 0.03, Misumi, Tokyo, Japan) were fixed near the center of the stationary glass plate of the PGPA keeping the distance between them at 19 mm and right above the objective lens of the microscope. The stationary bottom plate (110 × 200 × 1 mm thickness) of the PGPA was fixed to the microscope stage (IX71, Olympus, Tokyo, Japan).

RBC suspension, 8.5-μl, was then placed in the space between the two spacers on the glass plate, followed by placement of the upper moving glass plate (76 × 52 × 1.3 mm thick, S9213, Matsunami Glass, Osaka, Japan) apparatus over the blood sample, and finally connection of the slider block. The eccentric cam-motor system made the 2.5-mm stroke oscillation of the slider block using the 164-mm-long link system between the cam and the slider block. The ball bearings with tight fit, one on the slider block and the other on the cam, allowed smooth conversion of the motor rotation into sinusoidal movement of the slider block. The upper glass plate attached to the slider block slid on the surface of the stainless steel spacers, exerting a high shear stress on the RBCs kept in the space. The PGPA thus secured the space of 30 μm where RBC suspension could be exposed to a cyclically reversing shear stress.

The objective lens with 40× magnification (NA = 0.6, LCPlanFl 40×, Olympus) was used for imaging the RBCs. A high-speed video camera (MEMREMCAM fx-K3, Nac Image Technology, Tokyo, Japan) having a capability of 5000 frames/s with an exposure time of 1/20,000 s was attached to the microscope to capture the two-dimensional images of the RBCs. An

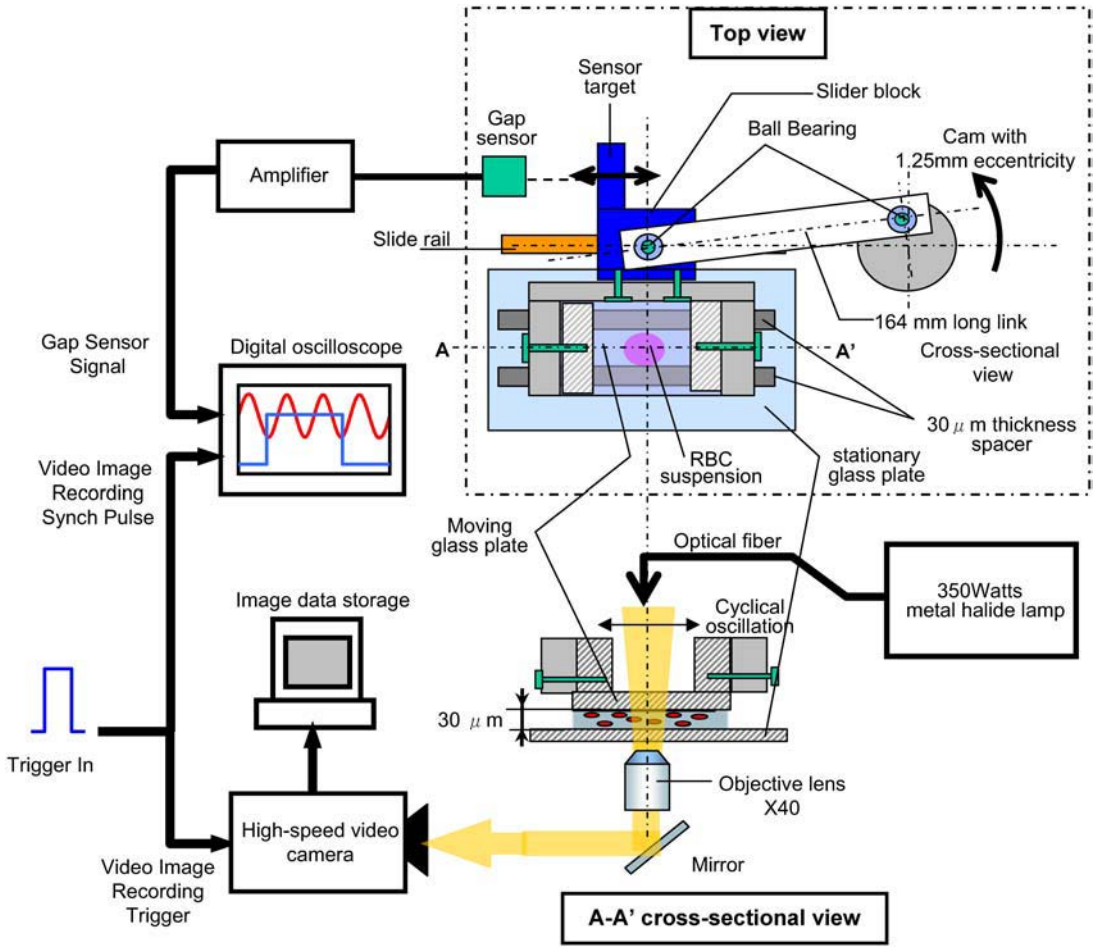

FIGURE 1 Schematic diagram of a CRSFG comprised of a slider-crank mechanism, a microscope data acquisition system, and a synchronized data acquisition system of RBC images with respect to a glass plate movement signal.

eddy-current gap sensor (PU-07, Applied Electronics, Kanagawa, Japan) fixed to the microscope stage detected the oscillating motion of the aluminum plate target attached to the slider block to provide continuous information on the glass plate movement.

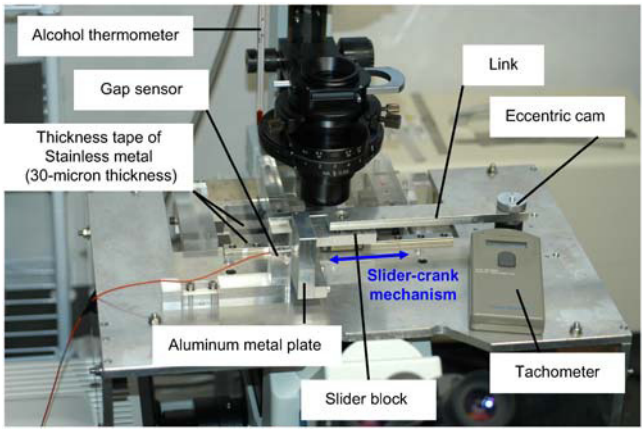

FIGURE 2 Assembled CRFGS showing the microscope stage mounted with a parallel glass plate assembly and a motor-cam system.

EXPERIMENTAL PROCEDURE

The cyclically reversing shear flow at the frequencies of 1, 2, 3, and 5 Hz (motor speed of 60, 120, 180, and 300 rpm) was generated using the CRSFG to exert the peak shear stress of ~53, 108, 161, and 274 Pa, respectively, to the RBC suspension. All the experiments were performed at a temperature of 24.5°C.

For image analysis, RBCs staying at around the midpoint between the two parallel glass plates were selected. The microscope focusing procedure was as follows: initially the microscope was focused on the bottom glass plate, followed by focusing on the top glass plate through manipulation of the dial gauge. When the two end points were determined manually, the dial gauge was then adjusted to the midpoint between the two end-points. In this way, RBCs staying at around the midpoint between the two parallel plates were selected for dynamic deformation analysis.

Manual trigger signal (see Fig. 1) started saving RBC images captured by a high-speed video camera in a personal computer, simultaneously digitizing and storing eddy-current gap sensor signal on a digital oscilloscope with the

sampling frequency of 10 kHz for a glass plate moving at 1 Hz, but a frequency of 20 kHz for those moving at 2, 3, and 5 Hz, respectively.

Data analysis

RBC image analysis 1; L/W ratio

Based on the image data with a resolution of 1280 × 200 pixels in an area of 0.38 × 0.06 mm, all the focused RBC images were analyzed in terms of the major (L) and minor (W) axes of the ellipsoidal shape. Previous workers have expressed RBC deformation in terms of either the L/W ratio (6,10) or the deformation index (DI) expressed by Eq. 11 (4–7,23,24):

$$DI = \frac{L - W}{L + W}. \tag{11}$$

The DI was originally derived by Taylor to describe the elongation patterns of the two-phase emulsion (30). Later, the DI was adopted for analysis of RBC deformation. The curves for DI versus shear stress, however, tend to flatten in the high-shear-stress region, losing resolution in the region >50 Pa. On the other hand, the L/W ratio is better suited to show the intersample difference in the high-shear-stress region. Since the objective of this study was to investigate the deformation response of RBCs to a cyclically reversing shear flow with an extremely high peak shear stress exceeding 100 Pa, we decided to employ the L/W as an index to quantify RBC deformation.

RBC image analysis 2; RBC velocity (V_{RBC})

At first, the center of the RBC image was determined from the intersecting point of the major and minor axes of the ellipsoidal image. The displacement of the RBC central point over three video frames was then measured to calculate the V_{RBC}, knowing that the elapsed time over three frames was 0.4 ms. The time course relation among the L/W, V_{RBC}, and glass plate velocity (V_{plate}) was then examined in each condition.

Location of the focused RBCs

The location of the RBCs focused between the two parallel glass plates was estimated assuming that the flow field between the two parallel glass plates was an oscillatory quasi-Couette flow. Based on the theory of oscillatory Couette flow (Materials and Methods), V_{RBC} varies in a sinusoidal manner. The ratio of V_{RBC} to V_{plate} can thus provide the approximate depth of the focused RBCs within the 30-μm clearance of the PGPA.

Derivation of V_{plate}

The temporal gap sensor signal was converted to yield the position data of the glass plate using the predetermined calibration data. Since the gap sensor signal contained white noise and since the derivation of V_{plate} involved computation of the first derivative of the position signal with respect to time, signal smoothing was employed to minimize noise enhancement. The moving average was repeated four times with different data samples each time. For the glass plate moving at 1 and 2 Hz, the first moving average involved 801 data points (400 data points before and after the current data point), the second 601 data points, the third 401 data points, and the fourth 201 data points. For the frequency of 3 Hz, 501, 401, 301, and 201data points were used, and finally, for the frequency of 5 Hz, 301, 101, 51, and 11 data points were used. The V_{plate} was then obtained using the following difference equation (Eq. 12), which was derived as the fourth-order approximation of the convection equation in the area of fluid dynamics (31).

$$U_0 = (D_{-2} - 8 \times D_{-1} + 8 \times D_1 - D_2)/(12\Delta t), \tag{12}$$

where U_0 is the plate velocity at current time 0, D_{-1}, D_{-2}, and D_1, D_2 are the smoothed-plate position data one and two data points before and after the current time, respectively, and Δt the sampling interval by oscilloscope. Δt is 0.0001 s for 1 Hz, whereas it is 0.00005 s for 2, 3, and 5 Hz of the plate velocity.

Estimation of the time-varying shear stress (τ)

The time-varying shear rate was obtained by dividing the V_{plate} by the clearance of 30 μm, followed by derivation of the time-varying shear stress (τ) by multiplying the shear rate with the viscosity of the suspension 0.200 Pa s. The time course changes of the relation between L/W and τ of RBCs were then analyzed.

RESULTS

Fig. 3, *a–d*, showed the sample images of RBCs for the cyclically reversing frequency of (*a*) 1 Hz, (*b*) 2 Hz, (*c*) 3 Hz, and (*d*) 5 Hz. For each frequency, the left panel (*i*) denoted RBC images with minimal L/W; the middle panel (*ii*) those at the zero shear stress (τ_0) when the V_{plate} was zero; and the right panel (*iii*) those with the maximal L/W. The RBCs were moving in the horizontal direction.

In Fig. 4, *a–d*, panel *i* showed the plate movement and its velocity for one second, panel *ii* the plate velocity and RBC velocity for one cycle, and panel *iii* the instantaneous shear stress and L/W of RBC during deformation and recovery phases. In the figures, the movement of the glass plate toward the right, away from the gap sensor on the microscope stage of Fig. 2, was denoted as the positive direction. The zero time in each figure denoted the moment when the glass plate was closest to the gap sensor, $V_{plate,zero}$ (τ_0). Both V_{RBC} and V_{plate} varied like sine waves. The correlation coefficients for the linear regressions between the V_{RBC} and V_{plate} signals was computed and shown in Fig. 5, *a–d*. Since the correlation coefficients between them were ~1.0, it could be said that the V_{RBC} followed the V_{plate} closely without any time lag, but with its amplitude being ~60% of the V_{plate} amplitude. The

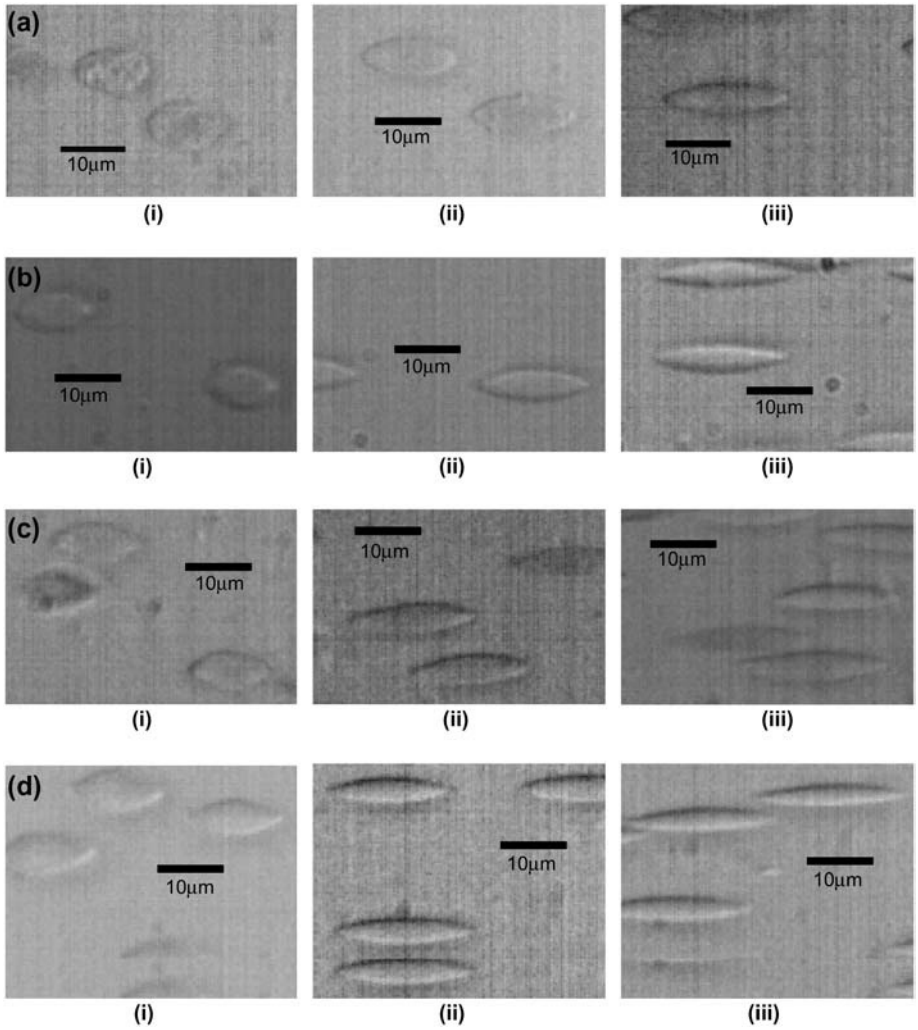

FIGURE 3 Typical RBC images under reversing shear flows. (*i*) Minimal elongation images, (*ii*) images remaining elongated when V_{plate} is zero (τ_0), and (*iii*) maximal elongation images under the reversing frequency of (*a*) 1 Hz, (*b*) 2 Hz, (*c*) 3 Hz, and (*d*) 5 Hz.

slope of the linear regression line *a* ($V_{RBC} = a \times V_{plate}$) between V_{RBC} and V_{plate} was 0.64, 0.57, 0.63, and 0.59 for 1, 2, 3, and 5 Hz, respectively, of plate frequency. The ratio of the V_{RBC} to the V_{plate} at the time of the maximal level of V_{plate} ($V_{plate,\ MAX}$) was 0.64 ± 0.07, 0.54 ± 0.05, 0.62 ± 0.04 and 0.59 ± 0.03 for 1 Hz, 2 Hz, 3 Hz, and 5 Hz, respectively, showing good agreement with the slopes of the linear regression lines. The RBC locations within the glass plates were then speculated to be 19.2, 17.1, 18.9, and 17.7 μm from the stationary bottom plate (Table 1) derived from the slopes of the linear regression equations of Fig. 5, *a–d*.

The *L/W* changes shown in Fig. 4, *a* (*iii*)–*d* (*iii*) did not follow the patterns of V_{plate} change exactly, but they showed asymmetrical response patterns consisting of fast deformation and slow recovery phase. The deformation phase was comprised of three periods: 1), a pre-rapid-elongation period lasting ~0.1 normalized fractional time (absolute time was normalized to one-cycle time); 2), rapid and linear elongation periods between 0.1 and 0.14 and between 0.6 and 0.64 of the normalized fractional time; and 3), a slow elongation period. The *L/W* during the rapid elongation period increased fairly linearly with time and shear stress (Fig. 6, *a* and *b*). During this period, the shear-stress level also increased linearly with time (Fig. 6 *c*). The slope of the linear regression lines with respect to time in Fig. 6 *a* increased from 34.9 to 89.4, 128.7, and 209.6/s, whereas those with respect to shear stress in Fig. 6 *b* decreased from 0.14 to 0.092, 0.066, and 0.039/Pa with the frequency.

Fig. 7 showed the mean *L/W* change rate during the rapid and linear elongation period (0.1 and 0.14 of the normalized cycle time) in comparison to the recovery period (0.46 and 0.58 of the normalized cycle time) as a function of the cyclically reversing frequency. The *L/W* change rates in both periods increased as a function of frequency, with the elongation rate more than twice the recovery rate.

An interesting finding was that dynamic *L/W* response lagged behind the shear-stress change during the shape recovery phase. The RBCs remained elongated even when the shear stress reached the zero level and continued to further decrease even after the shear stress started to increase in the other direction. Table 2 summarized the time lag. The mean lag time was 80 ms for 1 Hz, 40 ms for 2 Hz, 32 ms for 3 Hz,

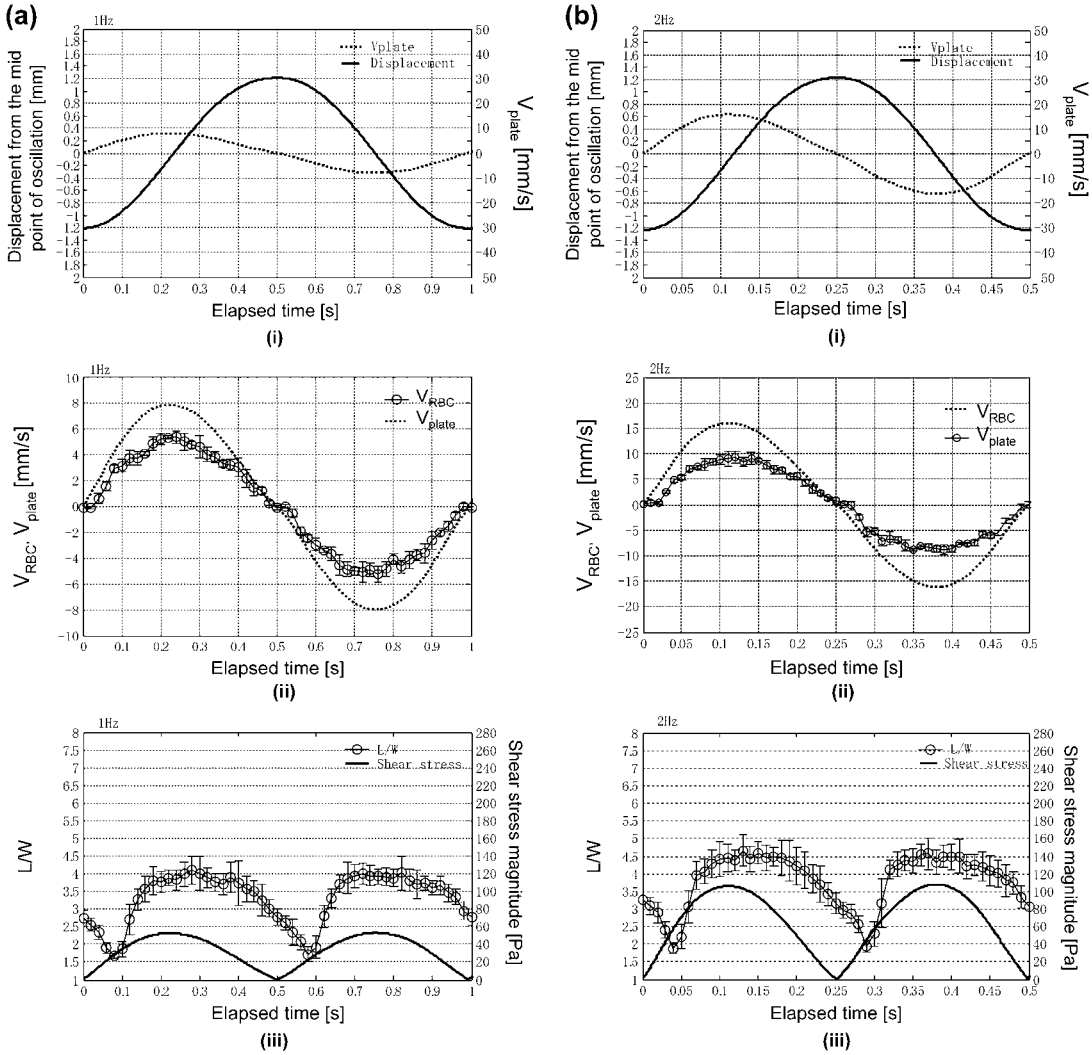

FIGURE 4 Time-course changes in the glass plate displacement, glass plate velocity V_{plate}, and RBC velocity V_{RBC}, generated shear stress, and RBC deformation L/W for reversing frequency of (*a*) 1 Hz, (*b*) 2 Hz, (*c*) 3 Hz, and (*d*) 5 Hz. For each frequency is shown (*i*) glass plate displacement and plate velocity V_{plate}, (*ii*) V_{plate} and V_{RBC}, and (*iii*) shear stress and L/W. The positive V_{plate} value indicates the glass plate motion toward the right in Fig. 2. In the figure, time 0 corresponds to when the slider block was closest to the gap sensor.

and 16 ms for 5 Hz, whereas the percent lag time normalized to one-cycle time was 8.0% for 1 Hz, 2 Hz, and 5 Hz, and 9.7% for 3 Hz.

In Fig. 8, the two-dimensional τ-L/W relationships of the data in Fig. 4 are shown. The shear stress τ was calculated by multiplying the time-varying shear rate by the fluid viscosity. The positive value of τ denoted that the flow was toward the right in Fig. 2. The τ-L/W patterns rotated in the counterclockwise direction in the right-half plane (the glass plate moving toward the right in Fig. 2), but in the clockwise direction in the left-half plane, showing the characteristic points for $V_{plate,zero}$ (*A*), L/W_{MIN} (*B* and *D*, respectively), and τ_{MAX} (*C* and *E*, respectively). The L/W_{MAX}, and L/W_{MIN} occurred twice in each cycle, one for either direction of the plate movement. Table 3 showed the numerical data for characteristic points on the τ-L/W curves. From Fig. 8, it was clear that the amplitude of L/W ($L/W_{AMP} = L/W_{MAX} - L/W_{MIN}$) increased with the cyclically reversing frequency. The value of L/W at the zero stress point τ_0 showed a tendency to increase from 2.77 ± 0.24 to 3.20 ± 0.30, 3.48 ± 0.33, and 4.44 ± 0.45 with the frequency.

Fig. 9 *a* shows the L/W_{MAX}, L/W_{MIN}, L/W at τ_0 (L/W_0), and L/W_{AMP} versus cyclically reversing frequency. The value of L/W_{MAX} increased from 4.06 ± 0.45 to 4.60 ± 0.33, 4.87 ± 0.46, and 6.34 ± 1.04, whereas L/W_{MIN} increased from 1.70 ± 0.14 to 1.81 ± 0.16, 2.16 ± 0.31, and 2.40 ± 0.24, and L/W_0 from 2.77 ± 0.14 to 3.20 ± 0.16, 3.48 ± 0.31, and 4.37 ± 0.24, respectively. Also shown in Fig. 9 *b* are DI_{MAX}, DI_{MIN}, DI_0, and DI_{AMP} ($DI_{MAX} - DI_{MIN}$) for the purpose of comparison with L/W. The DI value approached 1.0 and was not a sensitive indicator for shape change. In particular, DI_{AMP} decreased as the frequency increased.

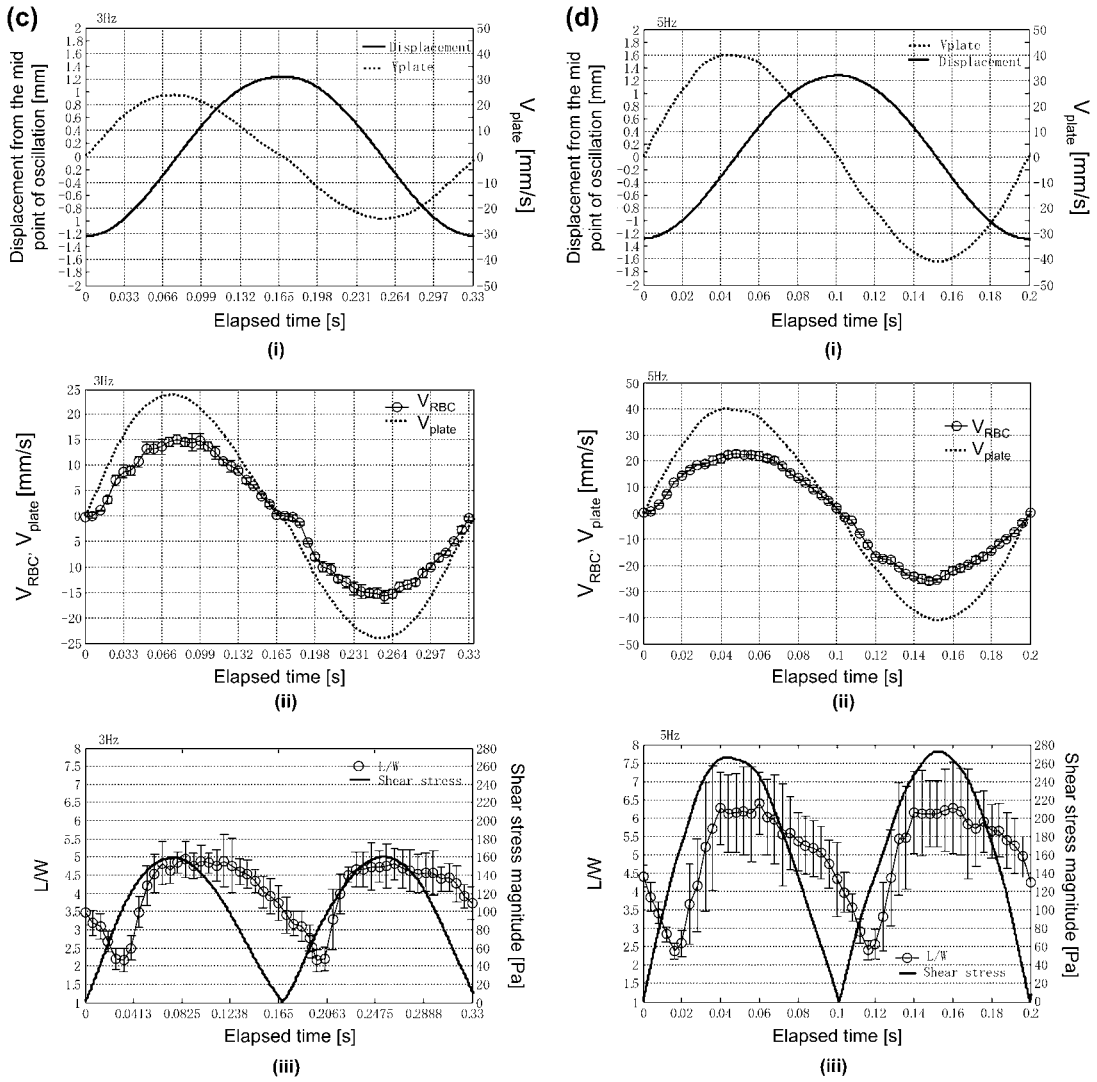

FIGURE 4 Continued

The L/W_{AMP} of RBCs normalized to the amplitude of τ (τ_{AMP}) was displayed in Fig. 10 *a*. As the reversing frequency increased, the frequency response expressed by the $L/W_{AMP}/\tau_{AMP}$ diminished. Likewise, DI_{AMP} normalized to the shear-stress amplitude also diminished with frequency (Fig. 10 *b*).

DISCUSSION

In this study, for the first time, the dynamic response of RBCs to a cyclically reversing shear flow with the peak shear stress level >100 Pa has been quantified using a specially built cyclically reversing shear flow generator. The validity of the results, however, depends on assumptions and questions related to the CRSFG system and data analysis. The first half of the discussion thus addresses the validation of 1), the stability of the PGPA, which is supposed to generate a quasi-Couette flow in the space of 30 μm; 2), the cell orientation in the shear-flow field; and 3), *L/W* as a parameter to express the deformation of RBCs. In the latter half of the discussion, the dynamic deformation and recovery response of RBCs to a cyclically reversing shear flow will be analyzed, and a simple model comprised of an elastic linear element for the deformation phase and a parallel combination of a spring and dashpot for the nonlinear recovery phase is proposed. The discussion also touches upon the shape recovery phenomenon in comparison to previous works, followed by future perspectives.

Validation and verification of the experimental conditions

Stability of the PGPA system and oscillatory quasi-Couette flow generation

In analyzing the dynamic response of RBCs to a cyclically reversing shear flow, we made an assumption that the flow

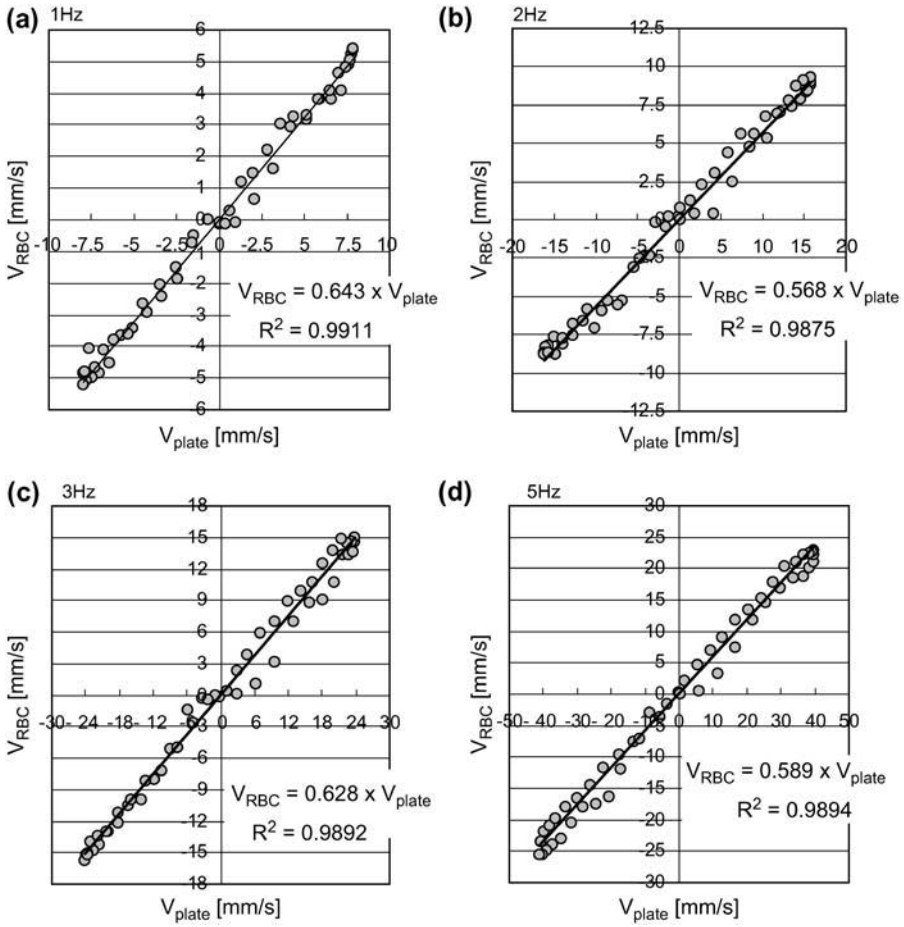

FIGURE 5 Linear regression analysis between V_{plate} and V_{RBC}. Hardly any time delay was observed between the two time-varying events.

field of RBC suspension between the two plates was steady and oscillatory quasi-Couette. The following three findings were obtained to verify the stability of the PGPA and the assumption of an oscillatory quasi-Couette flow. 1), The time course V_{RBC} measured at the midpoint in the PGPA showed the cyclic sinusoidal fluctuation with its amplitude ~0.60 of the V_{plate} (0.64 ± 0.07, 0.54 ± 0.05, 0.62 ± 0.04, and 0.59 ± 0.03 for 1 Hz, 2 Hz, 3 Hz, and 5 Hz, respectively) (Fig. 4 *a ii–d ii*, and Table 1). 2), The *L/W* of RBCs, both maximal and minimal levels, increased almost linearly as the reversing frequency increased (Fig. 9 *a*), indicating the stability of the PGPA over the frequency range between 1 and 5 Hz. 3), In addition, the V_{RBC} followed the V_{plate} without any time lag (Fig. 4, *a ii–d ii*, and linear regression analysis in Fig. 5, *a–d*). These three findings supported the stability of the PGPA and the theory that the CRSFG would successfully generate an oscillatory quasi-Couette flow in the 30-μm space of the PGPA.

Cell orientation

A question was raised concerning the accuracy of the dimensions of RBC images in the video frame because of cell orientation. RBCs may be randomly oriented under a reversing shear flow and the two-dimensional projected images may vary depending on the inclination level (5,10–13) of the RBCs in the flow field. The inclination level would change under the cyclically reversing shear flow. According to the reports by Keller and Skalak in 1982 (32) and Tran-Son-Tay in 1984 (10), the inclination level decreased when the

TABLE 1 Mean V_{RBC} amplitude, ratio of V_{RBC} to V_{plate}, and estimated RBC location from the bottom stationary plate for various glass plate reversing frequencies

Glass plate reversing frequency [Hz]	1	2	3	5
Mean of V_{RBC} amplitude [mm/s]	5.13 ± 0.58	8.69 ± 0.87	14.92 ± 0.89	24.15 ± 1.17
Ratio of V_{RBC} to V_{plate} at the time of $V_{plate,\ max}$	0.64 ± 0.07	0.54 ± 0.05	0.62 ± 0.04	0.59 ± 0.03
Averaged ratio of V_{RBC} to V_{plate}	0.64	0.57	0.63	0.59
Estimated location from stationary plate [μm]	19.2	17.1	18.9	17.7

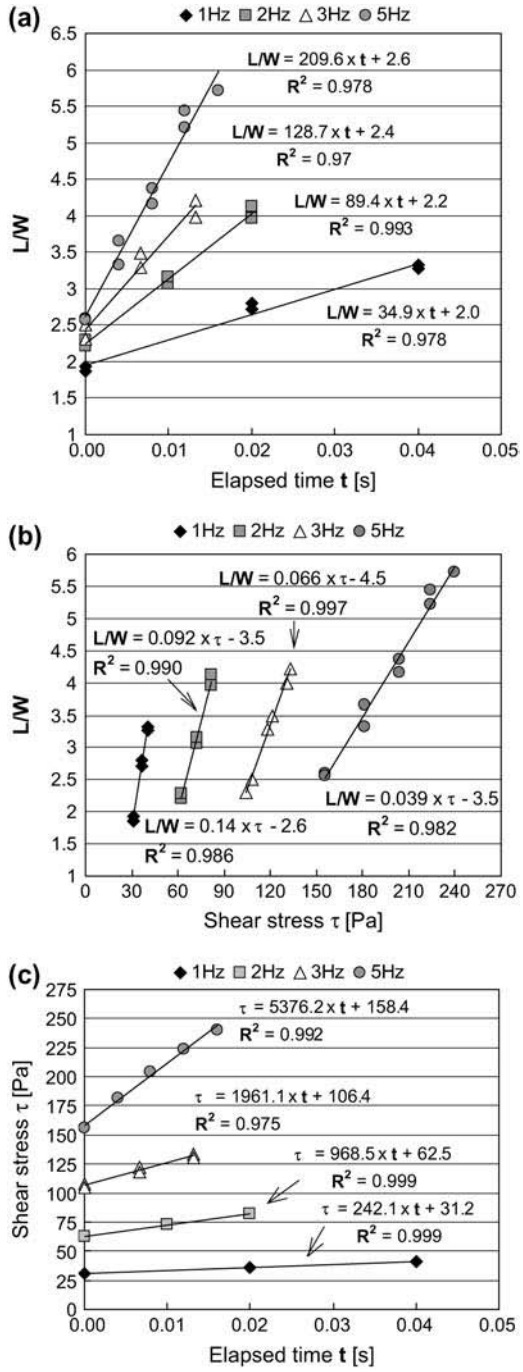

FIGURE 6 RBC responses in *L/W* during the rapid and linear elongation periods of the deformation phase. (*a*) *L/W* versus time; (*b*) *L/W* versus shear stress; and (*c*) shear stress versus time. During the rapid *L/W* increase period, *L/W* increased linearly to both time and the shear stress. The rapid and linear elongation periods occurred twice during each cycle at 0.1–0.14 and 0.6–0.64 s for 1 Hz, 0.05–0.07 and 0.3–0.32 s for 2 Hz, 0.0396–0.0528 and 0.2046–0.2178 s for 3 Hz, and 0.02–0.032 and 0.12–0.132 s for 5 Hz.

elongation level or shear rate of the RBCs increased. In our observation, since the membrane of the RBCs was always under some level of shear stress, the inclination problem was expected to be minimal. We observed some RBCs with their

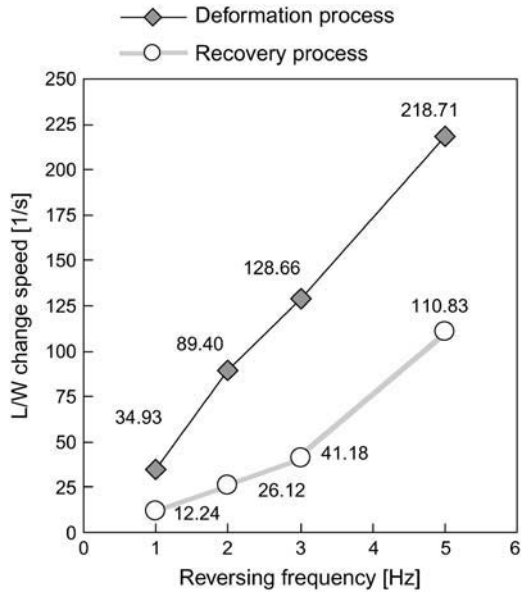

FIGURE 7 *L/W*-change speed during the deformation phase and the recovery phase. *L/W*-change speed was derived from the change in the absolute value of *L/W* with respect to time ($|d(L/W)|/dt$) during the rapid elongation period of the deformation phase (0.1–0.14 and 0.6–0.64 normalized time), and during the recovery phase (0.46–0.58 normalized time) of Fig 4, *a iii–d iii*.

shape partially out of focus right after their shapes returned to the minimal size under the oscillating frequency of 2 Hz and 3 Hz, whereas no specific events related to the orientation problem were observed at 1 Hz. In this study, therefore, special attention was paid to eliminate from data analysis those RBC images that were partially out of focus.

L/W versus DI

As for *L/W* to describe the dynamic responses of RBCs to a cyclically reversing shear flow with extremely high shear stress >100 Pa, the L/W_{MAX} and L/W_{MIN} values increased linearly with the increase in shear stress secondary to an increase in the reversing frequency (Fig. 9 *a*). The DI, however, did not provide a sensitive indication of the shape change, because it approached the value of 1.0. In particular, the DI_{AMP} decreased with the frequency in contrast to the L/W_{AMP}, which increased, although both amplitudes normalized to the input shear-stress amplitude diminished with the frequency (Fig. 9 *b*). From this standpoint, the selection of

TABLE 2 Absolute and normalized time delays averaged over one cycle time for various reversing frequencies

Glass plate reversing frequency [Hz]	1	2	3	5
Absolute time delay (mean value) [s]	0.080	0.040	0.032	0.016
Normalized time delay (mean value) [%]	8.0	8.0	9.7	8.0

Time delays were normalized from $V_{plate} = 0$ (τ_0) to L/W_{MIN} and are expressed in seconds and percentages for reversing frequencies of 1, 2, 3, and 5 Hz.

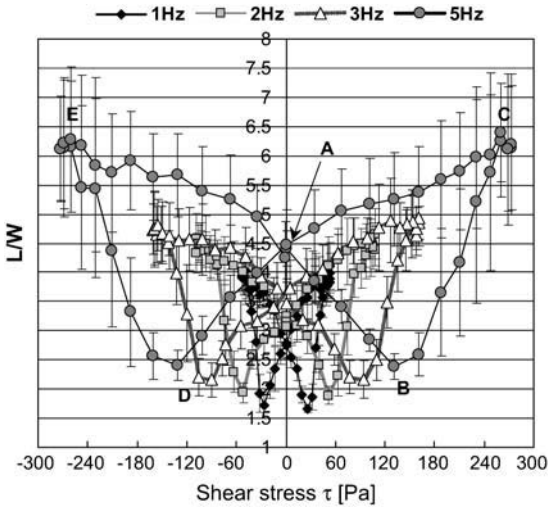

FIGURE 8 Two-dimensional display of shear stress versus L/W (τ-L/W) for reversing frequencies of 1, 2, 3, and 5Hz. The τ-L/W pattern rotated in the counterclockwise direction in the right-half plane, but in the clockwise direction in the left-half plane. Shown are the characteristic points for zero plate velocity (A), minimal L/W (B and D), and maximal shear stress (C and E).

L/W was the right decision for analyzing the shape change of RBCs at higher shear stress. Although the L/W showed better resolution than did the DI in describing a two-dimensional shape change of RBCs, it was only a ratio parameter between the longer and shorter axes assuming the RBC as an ellipsoidal shape. When the shape of the RBCs deviated from an ellipsoid at low shear stress as well as at extremely high shear stress, the L/W would fail to accurately represent the physical shape change. A better and more precise method of quantifying the morphological change of the RBCsunder varying shear stress would bring a better understanding of the RBC deformation and recovery process in a three-dimensional flow field.

Now the discussion will focus on the analysis of the dynamic RBC deformation and recovery under a cyclically reversing shear flow.

Dynamic response of RBCs to an oscillatory quasi-Couette shear flow

As for the response of RBCs to the oscillatory quasi-Couette shear flow, the L/W did not show sinusoidal fluctuations, although the time-course V_{RBC} and V_{plate} varied like sine curves (Fig. 4, *a–d*). The L/W showed asymmetrical response patterns comprised of a rapid deformation and a slow recovery phase. An interesting finding was that a time lag was observed between τ_0 and L/W_{MIN} (Fig. 4, *a iii–d iii*, and Tables 2 and 3). Additionally, the L/W_0 increased almost linearly with the frequency (Figs. 8 (zero-stress point *A*) and 9 *a*, and Table 3). The RBCs remained elongated and L/W continued to decrease even after the shear stress was reduced to zero and after the flow direction was reversed.

The two-dimensional display between L/W and τ as shown in Fig. 8 provided a better viewing of the dynamic deformation and recovery responses of RBCs to a cyclically reversing shear flow. The butterfly-like profiles of Fig. 8 were thought to represent the normal dynamic deformation and recovery processes of RBCs under a cyclically reversing shear flow. As the reversing frequency increased, the loop became extended in the horizontal direction, increasing the instantaneous stress and simultaneously shifting upward to a higher L/W level. The peak shear-stress level increased together with the L/W_{MAX} and L/W_{MIN}, and hence, the amplitude L/W_{AMP} became greater as the frequency increased.

Although the levels of the L/W_{MAX}, L/W_{MIN}, L/W_0, and L/W_{AMP} all increased with the frequency as shown in Fig. 9 *a*,

TABLE 3 Summary of normalized time (t/T), shear stress τ, and L/W at characteristic points on the τ-L/W curves

	Elapsed time t/T [−]				Shear stress τ [Pa]				L/W (mean ± SD)			
Characteristic point	1 Hz	2 Hz	3 Hz	5 Hz	1 Hz	2 Hz	3 Hz	5 Hz	1 Hz	2 Hz	3 Hz	5 Hz
(A)	0	0	0	0	0	0	0	0	2.75 ± 0.23	3.25 ± 0.31	3.47 ± 0.36	4.41 ± 0.30
(B)	0.08	0.08	0.033	0.08	25.8	52.1	33.2	131.8	1.67 ± 0.07	1.88 ± 0.15	2.16 ± 0.33	2.39 ± 0.22
(C)	0.25	0.25	0.25	0.25	53.5	108.1	161.2	273.7	3.99 ± 0.34	4.66 ± 0.44	4.93 ± 0.48	6.19 ± 1.20
(A)	0.5	0.5	0.5	0.5	0	0	0	0	2.78 ± 0.25	3.16 ± 0.30	3.73 ± 0.48	4.48 ± 0.60
(D)	0.58	0.58	0.594	0.58	25.8	52.1	33.2	131.8	1.73 ± 0.22	1.94 ± 0.17	2.15 ± 0.30	2.41 ± 0.26
(E)	0.75	0.75	0.75	0.75	53.5	108.1	161.2	273.7	3.95 ± 0.27	4.57 ± 0.44	4.74 ± 0.44	6.12 ± 0.89
(A)	1.0	1.0	1.0	1.0	53.5	108.1	161.2	273.7	2.78 ± 0.24	3.06 ± 0.25	3.74 ± 0.43	4.25 ± 0.62
Time elapsing direction	(A): Zero shear stress, when $V_{plate} = 0$ (B): Minimum L/W (L/W_{MIN}) (C): Maximum shear stress (τ_{MAX}) (A): Zero shear stress, when $V_{plate} = 0$ (D): Minimum L/W (L/W_{MIN}) (E): Maximum shear stress (τ_{MAX}) (A): Zero shear stress, when $V_{plate} = 0$											

Data in table refer to curves seen in Fig. 8. The data points are in the order A, B, C, A, D, E, and A, and data are expressed as mean ± SD for reversing frequencies of 1, 2, 3, and 5 Hz.

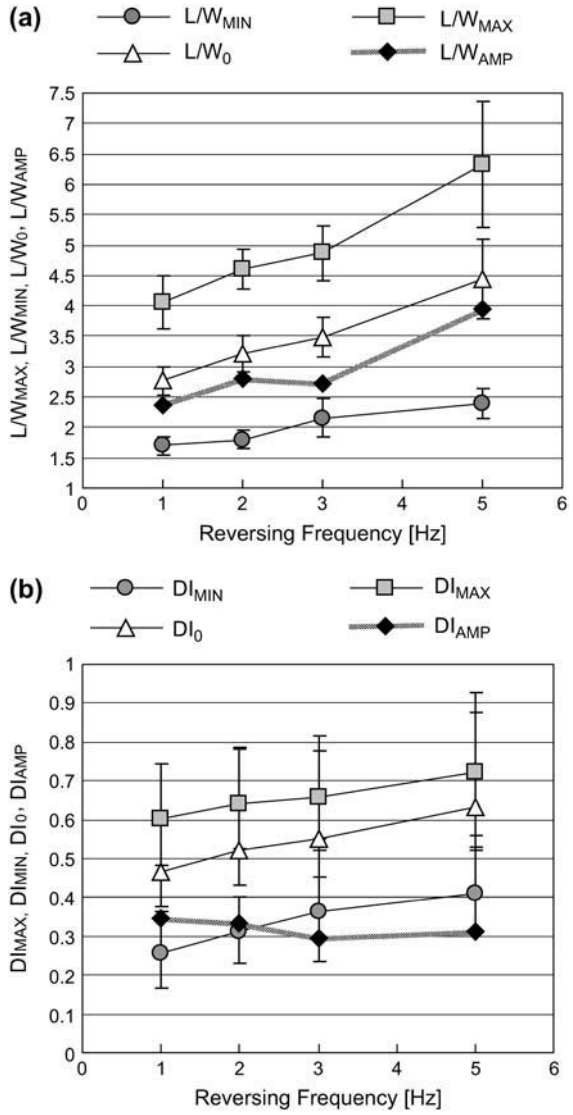

FIGURE 9 RBC deformation expressed in L/W and DI versus reversing frequency. (*a*) L/W_{MAX}, L/W_{MIN}, L/W_0, and L/W_{AMP} versus reversing frequency and (*b*) DI_{MAX}, DI_{MIN}, DI_0, and DI_{AMP} versus reversing frequency.

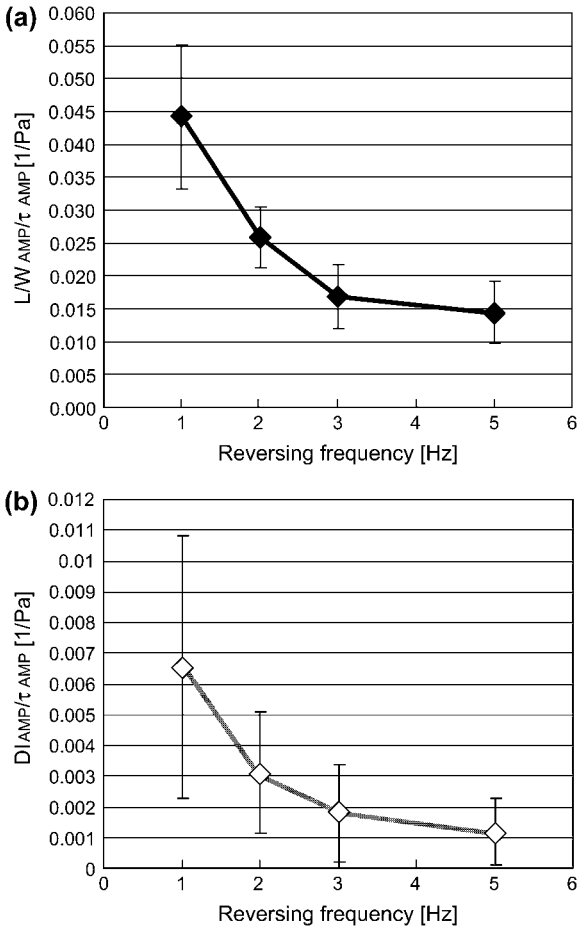

FIGURE 10 Frequency response of RBCs to reversing shear flow. (*a*) L/W_{AMP} normalized to τ_{AMP} versus reversing frequency and (*b*) DI_{AMP} normalized to τ_{AMP} versus reversing frequency.

the L/W_{AMP} normalized to τ_{AMP} decreased with the frequency, reaching a plateau at ~5 Hz (Fig. 10 *a*). Figs. 9 and 10 together disclosed that the RBCs continued to change their shape by increasing L/W in response to a cyclically reversing shear flow, but the normalized change of their L/W_{AMP} with respect to the shear-stress amplitude diminished upon reaching the plateau. The frequency response characteristics of RBC shape change to the reversing shear flow diminished with the frequency.

The deformation phase consisted of three periods: 1), a pre-rapid-elongation period lasting 0.1 normalized time unit; 2), rapid and linear elongation periods; and 3), a slow elongation period. During the rapid and linear elongation periods, L/W increased fairly linearly to both time and shear stress changes (Fig. 6, *a* and *b*). It should be noted that during this period, the shear stress increase rate was remarkably high with 242, 968, 1961, and 5376 Pa/s (Fig. 6 *c*). Regardless, the L/W increase was rather linear, exhibiting an elastic property. The slope of the linear regression lines ($d(L/W)/dt$) for the L/W-time relationships increased from 34.9 to 89.4, 128.7, and 209.6/s, whereas $d(L/W)/d\tau$ for the L/W-stress relationships decreased from 0.145 to 0.092, 0.049, and 0.040/Pa with the increase in frequency from 1 to 5 Hz. This result implies that the faster the shear rate, the faster is the RBC response in terms of L/W change, whereas the sensitivity of L/W change with respect to shear stress change diminishes if the initial L/W and shear levels are larger (Fig. 10 *a*).

Fig. 11 summarizes the characteristic points on the τ-L/W curves. Also shown are the speculated curves for the L/W versus steady uniform shear stress. Since the L/W increased linearly to the shear stress level during the rapid elongation period in our experiment (Fig. 6 *b*), but since the maximal L/W under the uniform shear cannot be attained under a cyclically reversing shear flow, particularly at higher reversing frequency, the L/W level in the steady uniform flow would be higher than the L/W_{MAX} of the reversing shear flow at

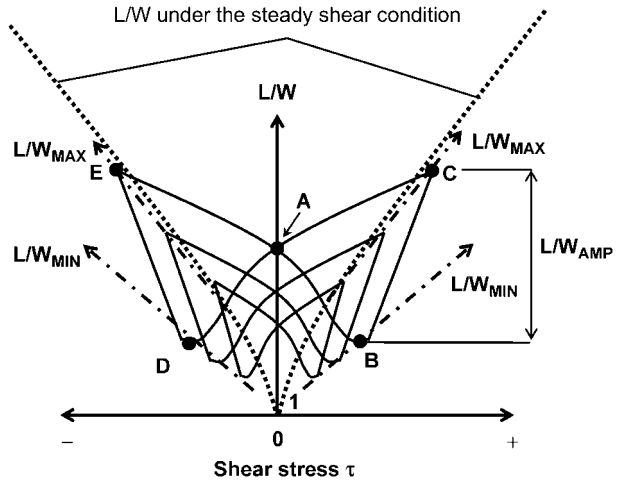

FIGURE 11 Shear stress-*L/W* plane display of RBC responses to reversing shear flows in comparison to the speculated response to the uniform shear flow.

higher frequency. The L/W_{MAX} of the reversing flow, however, should converge to that of the uniform shear flow at lower frequency.

An interesting finding was the lag time observed between the zero shear time and the L/W_{MIN} time. The RBCs remained elongated even if the external shear stress level returned to zero, and the *L/W* level continued to decrease for a little while even though the flow direction was reversed and the shear-stress level started to increase. At the time of zero shear stress, the energy stored in the RBC membranes to recover their original shape probably overrode the external tensional stress. The *L/W*, therefore, continued to decrease even though the external shear stress started to increase. As summarized in Table 2, ~8.0% of the time after the zero-shear-stress time for each frequency except 3 Hz (9.7%), the dynamic equilibrium between the intracellular recovery force and extracellular shear stress occurred to reverse the *L/W* change process. Further increase in the extracellular shear stress thus exceeded the cell's recovery force, and hence, RBCs started to elongate.

In the following section, a possible mechanical model to explain the dynamic response patterns of RBCs to a cyclically varying external shear flow is presented.

A simple mechanical model to explain dynamic RBC responses

Based on the experimental findings, a simple mechanical model as shown in Fig. 12 was proposed. The model consists of two phases, the deformation and recovery phases. The deformation phase consists of three periods: a pre-rapid-elongation period (Fig. 12 *a*, *S1*), a rapid elongation period (Fig. 12 *a*, *S2*), and a slow elongation period (Fig. 12 *a*, *S3*). An elastic linear element (Fig. 12 *b*) represents the rapid elongation period, and a parallel combination of a spring and dashpot (Fig. 12 *c*) represent the nonlinear recovery phase. A question was raised, however, concerning the validity of the model to describe the entire process of the deformation and recovery phase. To verify the validity of the model, the rapid elongation period was expressed as a constant-modulus model:

$$d\tau/dx = K,$$

where x is the displacement and K is the elastic modulus as obtained from the inverse of the slope in Fig. 6 *b*. Solving the above equation for τ, we obtain

$$\tau = Kx + C,$$

where C is the intercept of the shear-stress axis. Solving for displacement x, we obtain

$$x = (\tau - C)/K.$$

By substituting τ values from the experiment and initial shear-stress values for the linear portion, *L/W* curves were generated and are shown in Fig. 13. Although the model showed good agreement with the experimental data for the rapid elongation period, it deviated afterward from the experimental value as the shear-stress level increased. The deviation would possibly represent the alteration of the membrane elastic modulus depending on the membrane strain and shear-rate level, as reported by other workers (10,12).

Shape recovery phenomenon in comparison with the conventional reported studies

Previously reported studies of RBC shape recovery by Chien et al. (33), Hochmuth et al. (34), Sutera et al. (35), and Fischer (36) all concerned the response to a steplike removal of the constant tensional force applied to the cell membrane. On the other hand, the shape recovery shown in our study occurred under sinusoidal decrease of the extracellular shear level. The extracellular shear stress thus acted upon RBCs continuously by altering the tension level. This point is quite different from those of previous studies, where the applied force to RBCs was completely removed to observe the recovery process. As for the characteristics of the dynamic deformation of RBCs under cyclically reversing shear flow, Chien's study, that is, RBCs subjected to a steplike aspiration pressure and removal by a micropipette, has shown similar response patterns to our finding (33).

Future perspectives

The membrane moduli μ_m and η_m (where μ_m and η_m are the shear moduli of elasticity and shear viscosity, respectively) are variable, depending on shear stress and strain rate as well (10,12). These parameters were derived based on the energy balance between the input power (W_p) by extracellular shear

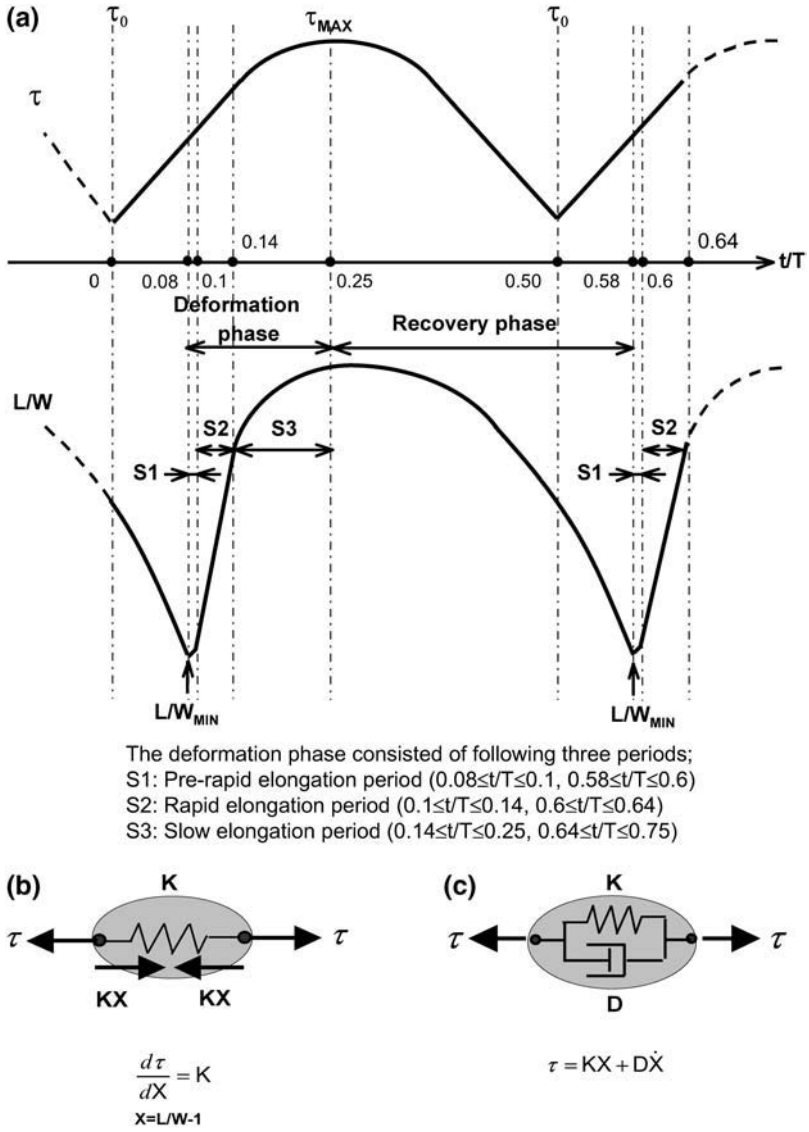

FIGURE 12 Analysis of RBC responses to reversing shear flows. (*a*) Time course asymmetric *L/W* changes showing deformation and recovery phases. The deformation phase consisted of three periods: *S1*, the pre-rapid-elongation period ($0.08 \le t/T \le 0.1$, $0.58 \le t/T \le 0.6$); *S2*, rapid and linear elongation periods: ($0.1 \le t/T \le 0.14$, $0.6 \le t/T \le 0.64$); and *S3*, slow and nonlinear elongation period ($0.14 \le t/T \le 0.25$, $0.64 \le t/T \le 0.75$). (*b*) Elastic element model representing the rapid and linear elongation period. (*c*) Viscoelastic element model representing the recovery phase.

condition, and the rate of energy dissipation in both the membrane (D_m) and cytoplasm (D_c). However, they were evaluated only under the steady shear condition (10,13). In the steady uniform flow condition, W_p would keep a constant value, whereas in our experiment, W_p would be variable under the varying shear flow. Consequently, the energy balance during the cycle would become variable and more complicated in comparison to the condition under the steady uniform shear flow. A more detailed theoretical consideration of RBC deformation under the reversing shear flow would require quantification of additional parameters, such as the tank-treading frequency and the effect of the ratio of intra- to extracellular viscosity.

The dynamic deformation behavior of RBCs as demonstrated in this study can be expected to occur in cardiovascular systems such as the heart chamber and narrow vessels, and prosthetic devices where shear stress varies from time to time and acts upon RBCs from all directions. The deformation and recovery responses under a varying shear flow may be different from cell to cell depending on their aging and pathophysiological states, including mechanical damages. The study of dynamic responses of various cells using our system will possibly clarify the pathophysiological status of blood cells related to various cardiovascular diseases and make preventive measures possible.

CONCLUSION

This study quantified the dynamic deformation and recovery responses of RBCs to a shear stress fluctuation with peak shear stress of 53, 108, 161, and 274 Pa using a cyclically reversing shear flow generator developed in our laboratory.

There were four important conclusions that could be drawn from this study. First, the V_{RBC} measured at around the

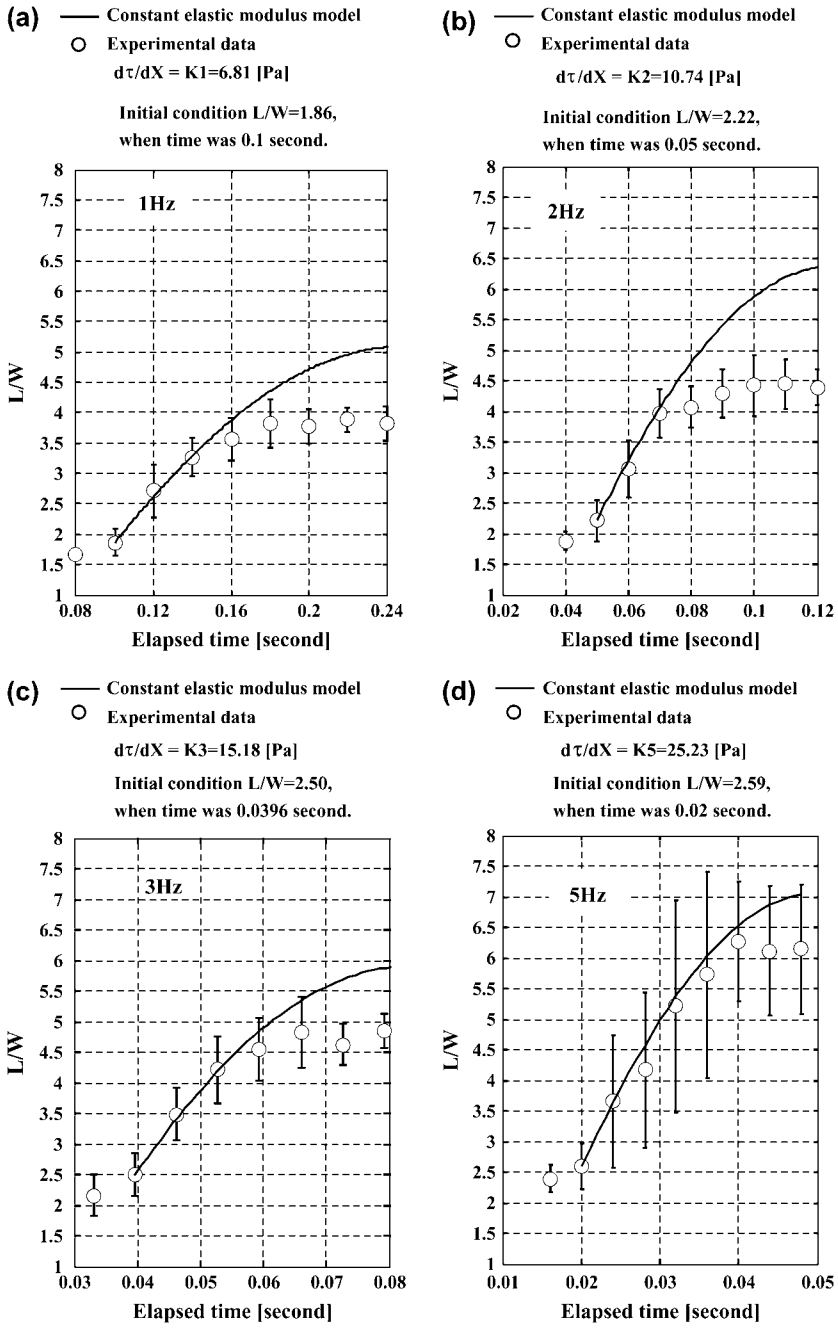

FIGURE 13 Analysis of the predictions based on the constant elastic modulus model versus experimental data during the deformation phase for (*a*) 1 Hz, (*b*) 2 Hz, (*c*) 3 Hz, and (*d*) 5 Hz.

midpoint of 30-μm parallel glass plate assembly followed the V_{plate} without any time delay with its amplitude ~60% of the V_{plate}. On the other hand, *L/W* consisted of a rapid deformation phase, and a nonlinear shape recovery phase. The deformation phase consisted of three periods: 1), a pre-rapid-elongation period; 2), rapid and linear elongation periods; and 3), a slow nonlinear elongation period. There was a time lag between L/W_{MIN} and τ_0, which was 8.0% of one cycle time, independent of the reversing frequency, for 1, 2, and 5 Hz; for 3 Hz, it was 9.7% of one cycle time.

Second, a simple mechanical model consisting of an elastic linear element during the rapid elongation period and a parallel combination of a spring and dashpot during the nonlinear recovery phase fit partially to describe dynamic deformation and recovery responses of RBCs to a cyclically reversing shear flow.

Third, the dynamic response behavior of RBCs under a cyclically reversing shear flow was different from the conventional shape change in which a steplike force is applied to and completely releases from the RBCs. The RBCs under a cyclically reversing shear flow are exposed to continuously varying shear flow to exhibit different dynamic responses.

Last, the current method was shown to be a simple approach for evaluating the RBC dynamic deformation and

recovery process in response to rapidly varying shear flows that simulates the flow patterns occurring in cardiovascular devices such as continuous-flow blood pumps.

We acknowledge the stimulating discussion of Associate Professor Hiroshi Mizunuma of Tokyo Metropolitan University, and Matsunami Glass Ind. of Tokyo, Japan, for their kind supply of material.

This study was partially supported by a grant-in-aid (14208103) to the principal investigator (S.T.) from the Japan Society for the Promotion of Science (JSPS). N.W. was supported by an Ishidu Shun Memorial Scholarship from April 2004 to March 2005 and by a research fellowship (17-3690) from the Japan Society for the Promotion of Science starting April 2005. N.W. is a Research Fellow (DC2) of the Japan Society for the Promotion of Science (JSPS).

REFERENCES

1. Skalak, R., and P.-I. Brånemark. 1969. Deformation of red blood cells in capillaries. *Science*. 164:717–719.
2. Schmid-Schönbein, H., and R. Wells. 1969. Fluid drop-like transition of erythrocytes under shear. *Science*. 165:288–291.
3. Fischer, T., and H. Schmid-Schönbein. 1977. Tank tread motion of red cell membranes in viscometric flow: behavior of intracellular and extracellular markers (with film). *Blood Cells*. 3:351–365.
4. Fischer, T. M., H. Schmid-Schönbein, and M. Stöhr-Liesen. 1978. The red cell as a fluid droplet: tank tread-like motion of the human erythrocyte membrane in shear flow. *Science*. 202:894–896.
5. Fischer, T. M., M. Stöhr, and H. Schmid-Schönbein. 1978. Red blood cell (RBC) microrheology: comparison of the behavior of single RBC and liquid droplets in shear flow. *Biorheology*. 74:38–45.
6. Pfafferott, C., G. B. Nash, and H. J. Meiselman. 1985. Red blood cell deformation in shear flow. Effects of internal and external phase viscosity and of in vivo aging. *Biophys. J*. 47:695–704.
7. Kon, K., N. Maeda, and T. Shiga. 1987. Erythrocyte deformation in shear flow: influences of internal viscosity, membrane stiffness, and hematocrit. *Blood*. 69:727–734.
8. Richardson, E. 1974. Deformation and haemolysis of red cells in shear flow. *Proc. R. Soc. Lond. A*. 338:129–153.
9. Sugihara, M., and H. Niimi. 1984. Numerical approach to the motion of a red blood cell in Couette flow. *Biorheology*. 21:735–749.
10. Tran-Son-Tay, R., S. P. Sutera, and P. R. Rao. 1984. Determination of red blood cell membrane viscosity from rheoscopic observations of tank-treading motion. *Biophys. J*. 46:65–72.
11. Niimi, H., and M. Sugihara. 1985. Cyclic loading on the red cell membrane in a shear flow: a possible cause of hemolysis. *J. Biomech. Eng*. 107:91–95.
12. Sutera, S. P., P. R. Pierre, and G. I. Zahalak. 1989. Deduction of intrinsic mechanical properties of the erythrocyte membrane from observations of tank-treading in the rheoscope. *Biorheology*. 26:177–197.
13. Tran-Son-Tay, R., S. P. Sutera, G. I. Zahalak, and P. R. Rao. 1987. Membrane stress and internal pressure in a red blood cell freely suspended in a shear flow. *Biophys. J*. 51:915–924.
14. Sutera, S. P. 1977. Flow-induced trauma to blood cells. *Circ. Res*. 41:2–8.
15. Leverett, L. B., J. D. Hellums, C. P. Alfrey, and E. C. Lynch. 1972. Red blood cell damage by shear stress. *Biophys. J*. 12:257–273.
16. MacCallum, R. N., E. C. Lynch, J. D. Hellums, and C. P. Jr. Alfrey. 1975. Fragility of abnormal erythrocytes evaluated by response to shear stress. *J. Lab. Clin. Med*. 85:67–74.
17. Heuser, G., and R. Opitz. 1980. A Couette viscometer for short time shearing of blood. *Biorheology*. 17:17–24.
18. Giersiepen, M., L. J. Wurzinger, R. Opitz, and H. Reul. 1990. Estimation of shear stress-related blood damage in heart valve prostheses: in vitro comparison of 25 aortic valves. *Int. J. Artif. Organs*. 13:300–306.
19. Paul, R., J. Apel, S. Klaus, F. Schügner, P. Schwindke, and H. Reul. 2003. Shear stress related blood damage in laminar Couette flow. *Artif. Organs*. 27:517–529.
20. Nevaril, C. G., E. C. Lynch, C. P. Jr. Alfrey, and J. D. Hellums. 1968. Erythrocyte damage and destruction induced by shear stress. *J. Lab. Clin. Med*. 71:784–790.
21. Velker, J. A., L. V. McIntire, and E. C. Lynch. 1977. Alteration of erythrocyte deformability due to shear stress as assessed by nucleoprotein filters. *Trans. Am. Soc. Artif. Intern. Organs*. 23:732–735.
22. Sandza, J. G., Jr., R. E. Clark, C. S. Weldon, and S. P. Sutera. 1974. Sub hemolytic trauma of erythrocytes: recognition and sequestration by the spleen as a function of shear. *Trans. Am. Soc. Artif. Intern. Organs*. 20:457–462.
23. Nakajima, T., K. Kon, N. Maeda, K. Tsunekawa, and T. Shiga. 1990. Deformation response of red blood cells in oscillatory shear flow. *Am. J. Physiol*. 259:H1071–H1078.
24. Kon, K., J. Murakami, K. Takaoka, and T. Shiga. 1988. Oscillatory deformation of human erythrocytes in sinusoidally modulated shear flow. *Biorheology*. 25:49–56.
25. Bludszuweit, C. 1995. Model for a general mechanical blood damage prediction. *Artif. Organs*. 19:583–589.
26. Bludszuweit, C. 1995. Three-dimensional numerical prediction of stress loading of blood particles in a centrifugal pump. *Artif. Organs*. 19:590–596.
27. Watanabe, N., T. Yasuda, H. Kataoka, and S. Takatani. 2004. Dynamic deformation capability of a red blood cell under a cyclically reciprocating shear stress. *Proc. 26th Annual Int. Conf. IEEE EMBS, San Francisco, CA*. 5069–5072.
28. Watanabe, N., Y. Arakawa, A. Sou, H. Kataoka, T. Yasuda, T. Fujimoto, and S. Takatani. 2005. Effects of shear stress and exposure time on RBC deformability as evaluated using an oscillatory Couette flow method. *Biorheology*. 42:153. (Abstr.)
29. Imai, I. 2003. Fluid Dynamics, Vol. I, 27th ed. Syokabo, Tokyo, Japan.
30. Taylor, G. I. 1934. The deformation of emulsions in definable fields of flow. *Proc. R. Soc. Lond. A*. 146:501–523.
31. Lomax, H., T. H. Pulliam, and D. W. Zingg. 2001. Fundamentals of Computational Fluid Dynamics. Scientific Computation. Springer, London.
32. Keller, S. R., and R. Skalak. 1982. Motion of a tank-treading ellipsoidal particle in a shear flow. *J. Fluid Mech*. 120:27–47.
33. Chien, S., K.-L. P. Sung, R. Skalak, S. Usami, and A. Tözeren. 1978. Theoretical and experimental studies on visco-elastic properties of erythrocyte membrane. *Biophys. J*. 24:463–487.
34. Hochmuth, R. M., P. R. Worthy, and E. A. Evans. 1979. Red cell extensional recovery and the determination of membrane viscosity. *Biophys. J*. 26:101–114.
35. Sutera, S. P., R. A. Gardner, C. W. Boylan, G. L. Carroll, K. C. Chang, J. S. Marvel, C. Kilo, B. Gonen, and J. R. Williamson. 1985. Age-related changes in deformability of human erythrocytes. *Blood*. 65: 275–282.
36. Fischer, T. M. 2004. Shape memory of human red blood cells. *Biophys. J*. 86:3304–3313.